

# Mathematical modelling for peristaltic transport of non-newtonian fluid through inclined non-uniform channel under the effect of surface roughness

Neeran Ammar<sup>a</sup>, Hayat A. Ali<sup>a,\*</sup>

<sup>a</sup>Department of Applied Science, University of Technology, Baghdad, Iraq

(Communicated by Javad Vahidi)

---

## Abstract

The effect of surface roughness on the peristaltic motion of a non-Newtonian Jeffery fluid down a non-uniform inclined channel was carried out, and the analysis has been investigated in two-dimensional channel Cartesian co-ordinates by using a low Reynolds number and a long-wavelength approximation, the governing equations (continuity, motion, and temperature) were modelled and then simplified. Mathematica 11.3 was used to find an analytical solution for the fluid flow i.e. fluid velocity, temperature, pressure gradient, pressure rise, and flow streamlines. The impact of interesting included parameters on axial velocity, stream function, temperature, pressure gradient, and pressure rise is graphically described.

Keywords: Peristaltic flow, Jeffrey fluid, Roughness surface.  
2020 MSC: 76B75

---

## 1 Introduction

Peristaltic transport has piqued researchers' interest for nearly five decades due to its physiological and industrial implications; as a result, a substantial study has been conducted in this field to understand the process of peristaltic pumping in engineering and physiological applications [6, 20, 27]. Material (slurry, solid-liquid mixture, or two immiscible liquids) is transferred from one point to another via peristaltic transport, which involves a continuous wave of area contraction and expansion over the length of an expandable duct or tube [6]. It involves the movement of matter in many body organs, including food in the gastrointestinal tract, urine transport to the bladder by the ureter, fluid in the cervical canal, ova transportation from the ovary to the uterus, fluid flow in the ductus deferens, lymph movement in lymphatic vessels, and blood flow in small blood vessels [20]. The above mechanism is employed in a variety of practical applications, including a heart-lung machine used during bypass surgery and a hemodialysis system. This pumping mechanism is also used to pump caustic chemicals, solidus liquids, slurry, and other fluids that require fluid isolation from the pump's moving elements [27]. The considerable literature on the subject of peristaltic transport can provide in-depth information on the issue. Latham [15] conducted the first investigation in this field, which was further extended by Shapiro et al. [26] and literature on peristaltic flows of various non-Newtonian fluids [10, 11, 12, 16, 17, 18, 28, 29, 32] and the references therein can be found.

---

\*Corresponding author

Email addresses: [as.20.22@grad.uotechnology.edu.iq](mailto:as.20.22@grad.uotechnology.edu.iq) (Neeran Ammar), [hayat.A.Ali@uotechnology.edu.iq](mailto:hayat.A.Ali@uotechnology.edu.iq) (Hayat A. Ali)

The study of non-Newtonian fluids has gotten a lot of interest because of its vast engineering and industrial applications, such as in physiology, fibre technology, material processing, shampoos, nuclear and chemical industries, oil reservoir engineering, and foodstuffs [1]. The nonlinear rheological properties of the non-Newtonian fluid are one of the essential aspects of its interest. Different models of non-Newtonian have been identified, among these models is Jeffrey fluid. It is a more straightforward linear model that relies on time derivatives rather than convected derivatives. Moreover, Jeffery's linear viscoelastic behaviour makes it more favorite in the polymer industries, blood flow and fluid mechanics. Further Jeffrey fluid considers a generalization of a Newtonian fluid i.e. Newtonian fluids reconsider as a special type of Jeffery's fluid [7]. Many researchers explored the significance linking of the peristalsis mechanism and Jeffrey fluid under various conditions. Lakshminarayana et al. [14] calculated the slip and heat transfer impact on the peristaltic flow of Jeffrey fluid in the porous medium through a vertical asymmetric channel. Hayat et al. [13] studied the peristaltic flow of MHD Jeffrey fluid in a curved channel, where the Soret and Dufour impact and convective conditions were discussed. Reddy et al. [24] examined the impact of several forces on the peristaltic flow of Jeffrey nanofluid in an asymmetric channel. Vajravelu et al. [30] analyzed the peristaltic flow of Jeffrey fluid in an inclined asymmetric channel. The properties of the Jeffrey fluid model for peristaltic chyme flow in the small intestine with a magnetic field were explored by Akbar et al. [3]. Akbar et al. [4] investigate the numerical solution of Williamson nanofluid flow in an asymmetric channel. The influence of the produced magnetic field and heat transfer on the peristaltic motion of a Jeffrey fluid in an asymmetric channel was discussed by Akram and Nadeem [5]. Ramesh [23] looked into the Jeffrey fluid and noted the effects of joule heating and viscosity dissipation. He proposed the exact solution under the influence of boundary slip conditions for plane Couette flow, generalized Couette flow, and plane Poiseuille flow. Abbasi et al. [2] investigated the MHD Jeffrey nanofluid. Mohammed R. Salman and Hayat A. Ali [25] investigate the heat transfer in an inclined tapered asymmetric porous channel for peristaltic flow of Jeffrey fluid with slip boundary conditions.

Surface roughness, often known as roughness, is a characteristic of surface texture. The deviations in the direction of a real surface's normal vector from its ideal form are used to quantify it. The surface is rough if these variances are considerable; the surface is smooth if they are minimal. Roughness is often thought of as the high-frequency, short-wavelength component of a measured surface in surface metrology. In practice, however, knowing both the amplitude and frequency is frequently required to confirm that a surface is suitable for a certain application. Roughness is critical in establishing how an actual thing interacts with its surroundings. Rough surfaces wear faster and have greater friction coefficients than smooth surfaces in tribology. Because abnormalities on the surface can act as nucleation sites for cracks or corrosion, roughness is often a strong predictor of a mechanical component's performance. In general, cross-scale descriptors such as surface factuality, rather than scale-specific descriptors, provide more relevant predictions of mechanical interactions at surfaces, such as contact stiffness [33] and static friction [9]. Nikolai V. Priezjev investigates the effect of molecular-scale surface roughness on slip behaviour in a flow of simple fluids driven by a constant force [22]. The fracture surface roughness that happens under mode is explained by Van Dam and De Pater [31]. To measure and compare the fractal dimension of the surface roughness profiles formed by laboratory hydraulic fracturing, Abbas Movassagh et al [19] used four fractal methods: compass, box-counting, variation, and roughness-length. Several natural rock fracture surfaces for which JRC has already been established are used to test the fractal model for fracture surfaces. The impact of scaling behaviour implied by a fractal is examined, as well as the relationship between fractal characterization and JRC. The nature of the fracture aperture space is described and examined [21].

To our knowledge, there has been no effort done to discuss the impact of surface roughness reactions on the peristaltic motion of a non-Newtonian fluid characterized by Jeffrey fluid flows through a non-uniform inclined channel which is practical in blood flow through stenosis arteries. The flow governing equations represented by continuity, movement, and temperature are mathematically constructed in a rectangle coordinates system. The long wavelength and low Reynolds number assumptions were employed to simplify the system into a system of differential equations which were solved analytically via the Mathematica program. The physical impact of various flow parameters on the velocity field, temperature, pressure gradient, pressure rise, and trapping phenomena are discussed graphically.

## 2 Problem Flow Mathematical Formulation

Let us consider the peristaltic flow of a non-Newtonian Jeffrey fluid through the non-uniform channel. The channel wall is supposed to have sinusoidal-shaped roughness. Assuming that the rectangular coordinate for the fixed frame is  $(\tilde{X}, \tilde{Y})$

The geometry of the wall surface is given as

$$\tilde{H}(\tilde{X}, \tilde{t}) = d(\tilde{X}) + b_1 \sin\left(\frac{2\pi}{L_1}(\tilde{X} - c\tilde{t})\right) - b_2 \cos^4\left(\frac{\pi\tilde{X}}{\tilde{\lambda}_1}\right) \quad (2.1)$$

With

$$d(\tilde{X}) = a + K\tilde{X} \quad (2.2)$$

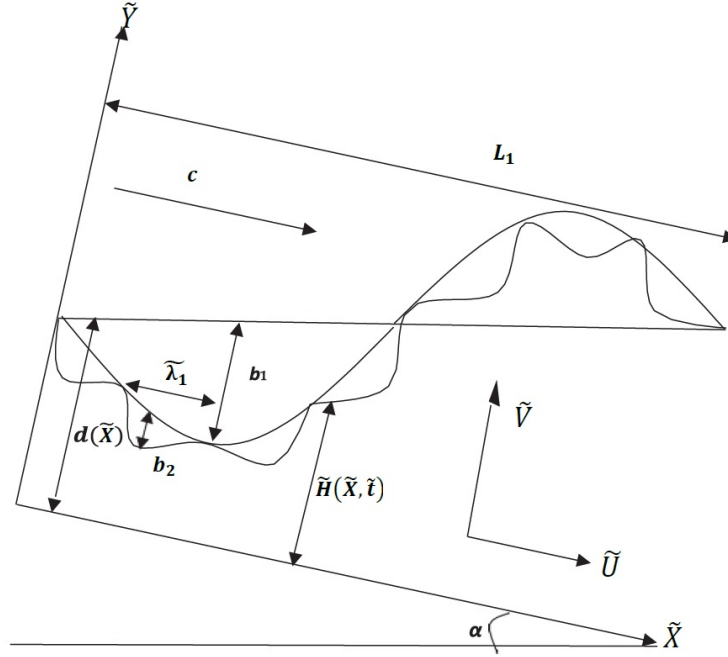


Figure 1: Geometry of the flow channel

where  $a$  is the half channel width at entry,  $b_1$  represent the amplitude,  $b_2$  is the roughness height,  $L_1$  is the wavelength,  $\tilde{\lambda}_1$  is the pitch,  $c$  is the wave propagation velocity,  $K$  is the non-uniformity parameter,  $\tilde{t}$  is the time and  $\tilde{X}$  is the axial variable.

The following equations governing the fluid flow in the laboratory frame of reference

The continuity equation has the form:

$$\frac{\partial \tilde{U}}{\partial \tilde{X}} + \frac{\partial \tilde{V}}{\partial \tilde{Y}} = 0 \quad (2.3)$$

and the momentum equations are

$$\rho \left( \frac{\partial \tilde{U}}{\partial \tilde{t}} + \tilde{U} \frac{\partial \tilde{U}}{\partial \tilde{X}} + \tilde{V} \frac{\partial \tilde{U}}{\partial \tilde{Y}} \right) = -\frac{\partial \tilde{P}}{\partial \tilde{X}} + \frac{\partial}{\partial \tilde{X}} (\tilde{S}_{\tilde{X}\tilde{X}}) + \frac{\partial}{\partial \tilde{Y}} (\tilde{S}_{\tilde{X}\tilde{Y}}) + \rho g \sin \alpha \quad (2.4)$$

$$\rho \left( \frac{\partial \tilde{V}}{\partial \tilde{t}} + \tilde{U} \frac{\partial \tilde{V}}{\partial \tilde{X}} + \tilde{V} \frac{\partial \tilde{V}}{\partial \tilde{Y}} \right) = -\frac{\partial \tilde{P}}{\partial \tilde{Y}} + \frac{\partial}{\partial \tilde{X}} (\tilde{S}_{\tilde{Y}\tilde{X}}) + \frac{\partial}{\partial \tilde{Y}} (\tilde{S}_{\tilde{Y}\tilde{Y}}) \quad (2.5)$$

Also, the energy equation has the form

$$\rho C_p \left( \frac{\partial \tilde{T}}{\partial \tilde{t}} + \tilde{U} \frac{\partial \tilde{T}}{\partial \tilde{X}} + \tilde{V} \frac{\partial \tilde{T}}{\partial \tilde{Y}} \right) = K \left( \frac{\partial^2 \tilde{T}}{\partial \tilde{X}^2} + \frac{\partial^2 \tilde{T}}{\partial \tilde{Y}^2} \right) + \tilde{S}_{\tilde{X}\tilde{X}} \frac{\partial \tilde{U}}{\partial \tilde{X}} + \tilde{S}_{\tilde{X}\tilde{Y}} \left( \frac{\partial \tilde{U}}{\partial \tilde{Y}} + \frac{\partial \tilde{V}}{\partial \tilde{X}} \right) + \tilde{S}_{\tilde{Y}\tilde{Y}} \frac{\partial \tilde{V}}{\partial \tilde{Y}} + \vartheta \quad (2.6)$$

where  $\tilde{U}, \tilde{V}, \rho, \tilde{T}, \tilde{P}, C_p, K, g, \vartheta$  are the laboratory frame velocity components, the fluid density, the temperature field, the pressure, the constant pressure specific heat, the electrical conductivity, gravitational acceleration, heat source and  $\tilde{S}_{\tilde{X}\tilde{X}}, \tilde{S}_{\tilde{X}\tilde{Y}}, \tilde{S}_{\tilde{Y}\tilde{X}}, \tilde{S}_{\tilde{Y}\tilde{Y}}$  represent the components of the extra stress tensor of Jeffery fluid which are derived as follows [25].

$$\tilde{S}_{ij} = \frac{1}{(1 + \lambda_1)}(\dot{\gamma} + \lambda_2 \ddot{\gamma}) \quad (2.7)$$

$$\dot{\gamma} = \nabla V + (\nabla V)^T \quad (2.8)$$

$$\ddot{\gamma} = \frac{\partial \dot{\gamma}}{\partial t} + (V \cdot \nabla) \dot{\gamma} \quad \text{where } (V \cdot \nabla) = \frac{\partial \tilde{U}}{\partial \tilde{X}} + \frac{\partial \tilde{V}}{\partial \tilde{Y}} \quad (2.9)$$

$\tilde{S}_{ij}$  represents the extra stress tensor ( $\lambda_1, \lambda_2$ ) is the Jeffrey parameters,  $\dot{\gamma}$  is the shear rate and dots over the quantities indicate differentiation concerning time, and  $\ddot{\gamma}$  is the second invariant strain tensor.

The associated relevant boundary conditions in the dimensional mathematical form are given below

$$\tilde{U} = 0 \quad \text{at} \quad \tilde{Y} = \tilde{H}, \quad \frac{\partial \tilde{U}}{\partial \tilde{Y}} = 0, \quad \text{at} \quad \tilde{Y} = 0 \quad (2.10)$$

$$\left[ \begin{array}{l} \tilde{T} = \tilde{T}_C \quad \text{at} \quad \tilde{Y} = 0 \\ \tilde{T} = \tilde{T}_W \quad \text{at} \quad \tilde{Y} = \tilde{H} \end{array} \right] \quad (2.11)$$

resistivity,  $\tilde{T}_C$  is the temperature at the centre of the channel,  $\tilde{T}_W$  is the temperature at the wall, and  $\alpha$  is the angle of inclination.

Introducing the following dimensionless transformations for facilitating the governing equations of the motion, as follows:

$$\begin{aligned} U &= \frac{\tilde{U}}{c}, \quad V = \frac{\tilde{V}}{c\delta}, \quad X = \frac{\tilde{X}}{L_1}, \quad Y = \frac{\tilde{Y}}{a}, \quad \theta = \frac{\tilde{T} - T_C}{T_W - T_C}, \quad Re = \frac{\rho c a_2}{\mu}, \quad S_{ij} = \frac{a}{\mu c} \tilde{S}_{ij}, \quad \delta = \frac{a}{L_1}, \quad \lambda_1 = \frac{\tilde{\lambda}_1}{L_1}, \quad t = \frac{c\tilde{t}}{L_1} \\ \tilde{P} &= \frac{a^2}{\lambda \mu c} \tilde{P}, \quad Pr = \frac{\mu C_p}{K}, \quad Ec_T = \frac{C^2}{(T_C - T_W)C_p}, \quad Ec_H = \frac{C^2}{(T_W - T_C)C_p}, \quad \theta_H = \frac{\tilde{T} - T_C}{T_W - T_C}, \quad h = \frac{H}{a}, \quad \theta_T = \frac{\tilde{T} - T_W}{T_C - T_W} \\ \epsilon &= \frac{K\lambda}{a}, \quad \Phi = \frac{b_1}{a}, \quad q = \frac{Q_o(X, t)}{ac}, \quad Q = \frac{\tilde{Q}}{ac}, \quad Fr = \frac{C^2}{ga_1}, \quad B = \frac{\vartheta a_2}{(T_W - T_C)K} \end{aligned} \quad (2.12)$$

Compensate Eq. (2.11) into Eqs. (2.1)–(2.10), leads to simplifying the equations into the following form

$$h = 1 + \epsilon x + \Phi \sin(2\pi(x - ct)) - \Phi_1 \cos^4\left(\frac{\pi x}{\lambda_1}\right) \quad (2.13)$$

$$\frac{\partial U}{\partial X} + \frac{\partial V}{\partial Y} = 0 \quad (2.14)$$

$$Re \delta \left( U \frac{\partial U}{\partial X} + V \frac{\partial U}{\partial Y} \right) = -\frac{\partial P}{\partial X} + \delta \frac{\partial}{\partial X} (S_{XX}) + \frac{\partial}{\partial Y} (S_{XY}) + \frac{Re}{Fr} \sin \alpha \quad (2.15)$$

$$Re \delta^3 \left( U \frac{\partial V}{\partial X} + V \frac{\partial V}{\partial Y} \right) = -\frac{\partial P}{\partial X} + \delta^2 \frac{\partial}{\partial X} (S_{YX}) + \delta \frac{\partial}{\partial Y} (S_{YY}) \quad (2.16)$$

$$Re Pr \delta \left( U \frac{\partial \theta_T}{\partial X} + V \frac{\partial \theta_T}{\partial Y} \right) = \delta^2 \frac{\partial^2 \theta_T}{\partial X^2} + \frac{\partial^2 \theta_T}{\partial Y^2} + Ec_T Pr \left( \delta \frac{\partial U}{\partial X} S_{XX} + \frac{\partial U}{\partial Y} S_{XY} + \delta^2 \frac{\partial V}{\partial X} S_{XY} + \delta \frac{\partial V}{\partial Y} S_{YY} \right) + B \quad (2.17)$$

$$Re Pr \delta \left( U \frac{\partial \theta_H}{\partial X} + V \frac{\partial \theta_H}{\partial Y} \right) = \delta^2 \frac{\partial^2 \theta_H}{\partial X^2} + \frac{\partial^2 \theta_H}{\partial Y^2} + Ec_H Pr \left( \delta \frac{\partial U}{\partial X} S_{XX} + \frac{\partial U}{\partial Y} S_{XY} + \delta^2 \frac{\partial V}{\partial X} S_{XY} + \delta \frac{\partial V}{\partial Y} S_{YY} \right) + B \quad (2.18)$$

$$S_{XX} = \frac{2\delta\mu}{(1+\lambda_1)} \left( 1 + \frac{c\delta\lambda_2}{a} \left( \frac{\partial U}{\partial X} + \frac{\partial V}{\partial Y} \right) \right) \frac{\partial U}{\partial X} \quad (2.19)$$

$$S_{XY} = S_{YX} = \frac{\mu}{(1+\lambda_1)} \left( 1 + \frac{c\delta\lambda_2}{a} \left( \frac{\partial U}{\partial X} + \frac{\partial V}{\partial Y} \right) \right) \left( \frac{\partial U}{\partial Y} + \delta^2 \frac{\partial V}{\partial X} \right) \quad (2.20)$$

$$S_{YY} = \frac{2\delta\mu}{(1+\lambda_1)} \left( 1 + \frac{c\delta\lambda_2}{a} \left( \frac{\partial U}{\partial X} + \frac{\partial V}{\partial Y} \right) \right) \frac{\partial V}{\partial Y} \quad (2.21)$$

Moreover, the instantaneous flow rate between the centre line and the wall is determined by

$$Q_o(X, t) = \int_0^{H(X)} \tilde{U}(\tilde{Y}) d\tilde{Y} \quad (2.22)$$

Suppose that  $Q_o(X, t)$  periodic in  $(X - t)$ , and using the dimensionless quantity listed in Eq. (2.11), the dimensionless form of flow flux is [8]

$$q(X, t) = Q + \phi \sin 2\pi(X - t) \quad (2.23)$$

where  $Re$  is the Reynolds number,  $U$  and  $V$  are the velocity components for  $(X, Y)$  directions,  $\delta$  is the wavenumber,  $T_C$  is the temperature at the centre of the channel,  $T_W$  is the temperature at the wall,  $Pr$  is the Prandtl number,  $\theta_H$  is the dimensionless in the case of uniform heat flux,  $\theta_T$  is the dimensionless in the case of uniform surface temperature,  $Ec_H$  is the Eckert number in the case of uniform heat flux,  $Ec_T$  is the Eckert number in the case of uniform surface temperature, and  $K$  is the thermal conductivity,  $\tilde{Q}$  is the time-mean flow over one period of the wave, and  $q(X, t)$  is the flow rate in the wave frame.

Adopting the assumption of long-wavelength  $\delta \ll 1$  and low Reynolds number Eqs. (2.14)–(2.20) reduced to the forms

$$\frac{\partial P}{\partial X} = \frac{\partial}{\partial Y}(S_{XY}) + \frac{Re}{Fr} \sin \alpha \quad (2.24)$$

$$\frac{\partial P}{\partial Y} = 0 \quad (2.25)$$

$$\frac{\partial^2 \theta_T}{\partial Y^2} + Ec_T Pr \frac{\partial U}{\partial Y} S_{XY} + B = 0 \quad (2.26)$$

$$\frac{\partial^2 \theta_H}{\partial Y^2} + Ec_H Pr \frac{\partial U}{\partial Y} S_{XY} + B = 0 \quad (2.27)$$

combined with the dimensionless boundary conditions:

$$U = 0 \text{ at } Y = h, \quad \frac{\partial U}{\partial Y} = 0 \text{ at } Y = 0 \quad (2.28)$$

$$\begin{bmatrix} \theta_H = 0, \theta_T = 1 \text{ at } Y = 0 \\ \theta_H = 1, \theta_T = 0 \text{ at } Y = h \end{bmatrix} \quad (2.29)$$

where

$$S_{XY} = S_{YX} = \frac{\mu}{(1+\lambda_1)} \frac{\partial U}{\partial Y}, \text{ and } S_{XX} = S_{YY} = 0 \quad (2.30)$$

### 3 Solution of the problem

The system of motion and temperature Eqs. (2.23), (2.25) and (2.26) are solved analytically with the help of MATHEMATIC under suitable boundary conditions in Eqs. (2.27), and (2.28).

The explicit expressions for the solutions of  $U$ ,  $\theta_T$  and  $\theta_H$  respectively are

$$U(y) = \frac{1}{2Fr} - \frac{dp}{dX} Frh^2 + \frac{dp}{dX} Fr y^2 + \frac{dp^2}{dX} Re \sin(\alpha) - Rey^2 \sin(\alpha) - \frac{dp}{dX} Frh^2 \lambda_1 + \frac{dp}{dX} Fr y^2 \lambda_1 + h^2 Re \sin(\alpha) \lambda_1 - Rey^2 \sin(\alpha) \lambda_1$$

$$\begin{aligned} \theta_H(y) = & \frac{1}{12Fr^2h} (12Fr^2y + 6BFr^2h^2y - 6BFr^2h^2y + \frac{dp^2}{dX} Fr^2h^4 Pr y Ec_H - 2 \frac{dp}{dX} Frh^4 Pr Rey \sin(\alpha) Ec_H \\ & + 2 \frac{dp}{dX} Frh Pr Rey^4 \sin(\alpha) Ec_H + h^4 Pr Re^2 y \sin(\alpha)^2 Ec_H - h Pr Re^2 y^4 \sin(\alpha)^2 Ec_H \\ & + \frac{dp^2}{dX} Fr^2h^4 Pr y Ec_H \lambda_1 - \frac{dp^2}{dX} Fr^2h Pr y^4 Ec_H \lambda_1 - 2 \frac{dp}{dX} Frh^4 Pr Rey \sin(\alpha) Ec_H \lambda_1 \\ & + 2 \frac{dp}{dX} Frh Pr Rey^4 \sin(\alpha) Ec_H \lambda_1 + h^4 Pr Re^2 y \sin(\alpha)^2 Ec_H \lambda_1 - h Pr Re^2 y^4 \sin(\alpha)^2 Ec_H \lambda_1) \end{aligned}$$

$$\begin{aligned} \theta_T(y) = & \frac{1}{12Fr^2h} (12Fr^2h - 12BFr^2y + 6BFr^2h^2y - 6BFr^2h^2y + \frac{dp^2}{dX} Fr^2h^4 Pr y Ec_T - \frac{dp^2}{dX} Fr^2h Pr y^4 Ec_T \\ & - 2 \frac{dp}{dX} Frh^4 Pr Rey \sin(\alpha) Ec_T + 2 \frac{dp}{dX} Frh Pr Rey^4 \sin(\alpha) Ec_T + h^4 Pr Re^2 y \sin(\alpha)^2 Ec_T \\ & - h Pr Re^2 y^4 \sin(\alpha)^2 Ec_T + \frac{dp^2}{dX} Fr^2h^4 Pr y Ec_T \lambda_1 - \frac{dp^2}{dX} Fr^2h Pr y^4 Ec_T \lambda_1 - 2 \frac{dp}{dX} Frh^4 Pr Rey \sin(\alpha) Ec_T \lambda_1 \\ & + 2 \frac{dp}{dX} Frh Pr Rey^4 \sin(\alpha) Ec_T \lambda_1 + h^4 Pr Re^2 y \sin(\alpha)^2 Ec_T \lambda_1 - h Pr Re^2 y^4 \sin(\alpha)^2 Ec_T \lambda_1) \end{aligned}$$

Then from Eq. (2.23), we get the gradient of pressure  $\frac{dp}{dX}$  as follows

$$\frac{dp}{dX} = \frac{-3q(X, t)}{(1 + \lambda_1)h^3} + \frac{Re \sin(\alpha)}{Fr} \quad (3.1)$$

and the dimensionless pressure rise  $\Delta P$  across the channel of unit length is given as

$$\Delta P = \int_0^1 \frac{dp}{dX} dX. \quad (3.2)$$

## 4 Graphical Results and Discussion

In this section, we have presented the graphical results and the physical interpretation of various flow interesting parameters on velocity profile, temperature distribution, pressure gradient and pressure rise.

### 4.1 Velocity Profile

Figures 2(a)-(d) depict the axial velocity profile  $U(y)$  in the y-direction for a nonuniform channel due to the effects of the volume of Jeffrey fluid parameter  $\lambda_1$ , flow rate  $Q$ , amplitude ratio  $\Phi$  and the roughness parameter  $\Phi_1$ . Figures 2(a)-(d) show that for non-uniform channels, the maximum velocity is obtained at the centerline and decreases as the channel approaches the wall. Figure 2(a) is plotted to describe the effect of  $\lambda_1$  on velocity profile. The figure appears that there is no effect of  $\lambda_1$  on velocity profile. Figures 2(b), 2(c) and 2(d) are prepared to see the variation of  $Q$ ,  $\Phi$  and  $\Phi_1$  respectively on velocity profile. It can be noticed that a rise in  $Q$  lead to an increment in velocity. Along the channel length, there is an elevation impact  $\Phi$  on  $u(y)$ , whereas the central region of the channel decreases along the length of the channel, near the middle of the non-uniform channel. The velocity of the fluid rises via a steady increase in the roughness parameter  $\Phi_1$  value, while diminishing the effect for  $\Phi_1$  indicating near the channel walls.

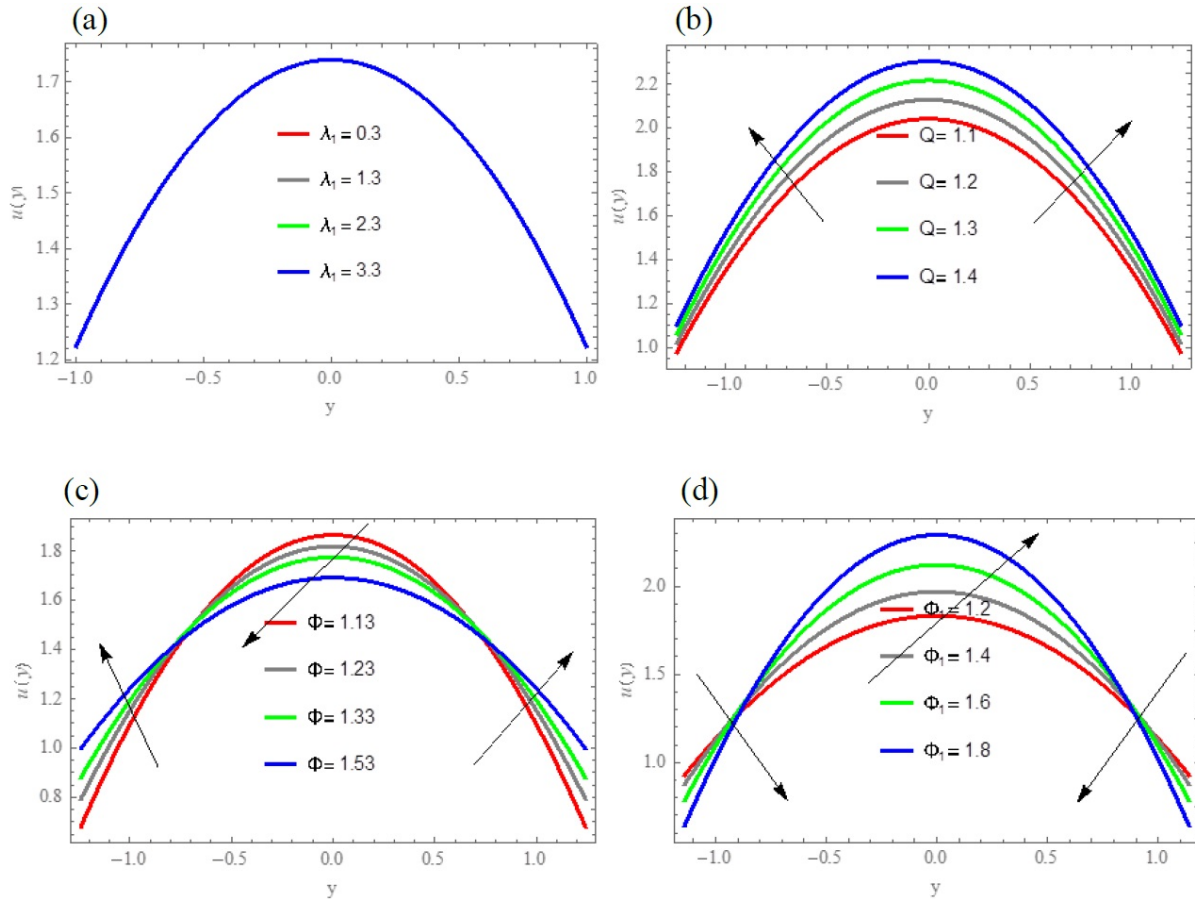


Figure 2: Velocity profile for different values of (a) Jeffrey fluid parameter  $\lambda_1$  (b) flow rate  $Q$  (c) amplitude ratio  $\Phi$  (d) roughness parameter  $\Phi_1$  and for fixed values of parameters  $\{Fr = 1.2, Re = 0.5, x = 0.4, \alpha = 0.3, t = 0.1, L_1 = 2.1\}$

## 4.2 Temperature distribution

Figures 3 and 4 show how the amplitude ratio  $\Phi$  and surface roughness parameters  $\Phi_1$  affect the temperature distribution for various values of the surface roughness and all other parameters, whereas Figures 5 and 6 show how Jeffrey fluid parameter  $\lambda_1$  and the Eckert number affects the temperature distribution for various values of the surface roughness and all other parameters. The preceding analysis was completed under two conditions: uniform heat flux  $\theta_H(y)$  and uniform surface  $\theta_T(y)$  temperature. The change in  $\theta_H(y)$  for various values  $\Phi$  is seen in Figure 3(a).  $\theta_H(y)$  moves from a maximum value on the right side of the channel wall to a minimum value on the left side of the channel wall as  $\Phi$  increases, Figure 3(b) depicts the variance in  $\theta_T$  versus  $y$  for various values of  $\Phi$ . As we can see, the value of  $\theta_T(y)$  increase as the value  $\Phi$  increases, till reaches stable values near the central part of the non-uniform channel. Figures 4(a) and 4(b) demonstrate the temperature profile for various values of surface roughness parameters for both the uniform heat flux and uniform surface temperature boundary conditions discussed previously. Two different reactions of surface roughness impact on  $\theta_H(y)$  are seen, i.e. moving from a maximum value on the left side of the region ( $0.7 \leq y \leq 1.4$ ) of the channel wall to a significant dip of the right side of the region ( $1.5 \leq y \leq 2.5$ ) of the channel wall, whereas the effect of surface roughness on  $\theta_T(y)$  have the same impact from the left side While the difference on the right side is merely a minor drop, Figures 5(a), and (b) demonstrate the effect of Jeffrey fluid parameter  $\lambda_1$  on both  $\theta_H(y)$  and  $\theta_T(y)$  which can see from Figure 5(a) that the effect of  $\lambda_1$  on  $\theta_H(y)$  is the same as the effect  $\Phi$  which means moves from a maximum value on the right side of the channel wall to a minimum value on the left side of the channel wall as  $\lambda_1$  increases also Figure 5(b) has the same effect of  $\lambda_1$  on  $\theta_T(y)$  which means the value of  $\lambda_1$  increase as the value of  $\theta_T(y)$  rises, and there is no influence of  $\lambda_1$  in the centre of the non-uniform channel. As seen in Figure 6(a) there are two impacts of  $Ec$  on  $\theta_H(y)$  where we can notice that there is a slight rise is almost non-existent from the left side while a clear decrease can be observed on the right side of  $\theta_H(y)$  on the non-uniform channel wall. Figure 6(b) clarifies a raise in  $Ec_T$  causing a rise in the  $\theta_T(y)$ .

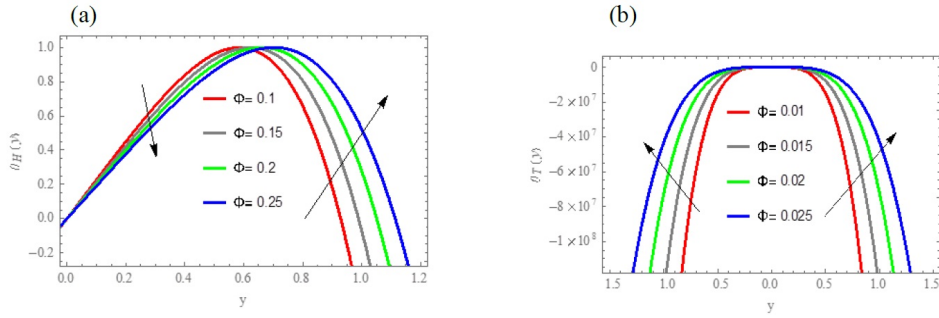


Figure 3: Temperature profile with various values of  $\Phi$  at  $\{Fr = 1.5, Re = 1.5, x = 0.2, \alpha = 0.1, \lambda_1 = 0.2, \epsilon = 0.1, Q = 0.3, \Phi_1 = 1.2, t = 0.1, L_1 = 2.1, Pr = 1., Ec_T = 1.1, B = 0.1\}$  (a) uniform heat flux condition (b) uniform surface temperature

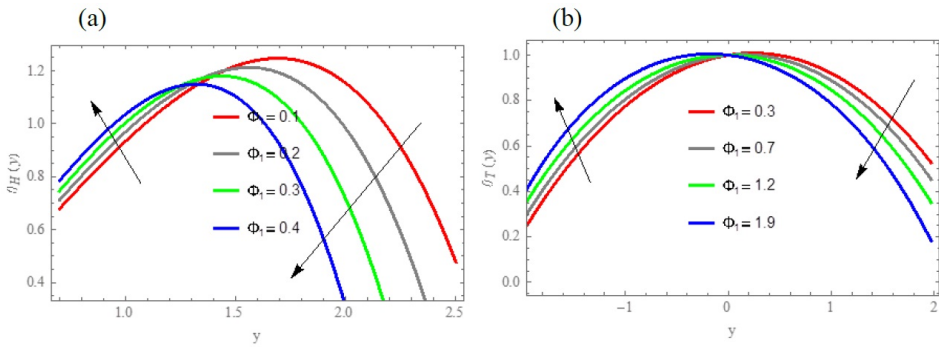


Figure 4: Temperature profile with various values of  $\Phi_1$  at  $\{Fr = 1.5, Re = 1.5, x = 0.25, \alpha = 0.1, \lambda_1 = 0.4, \epsilon = 0.31, Q = 1.3, \Phi = 2.1, t = 0.1, L_1 = 1.1, Pr = 0.42, Ec_T = 0.42, B = 0.3\}$  (a) uniform heat flux condition (b) uniform surface temperature

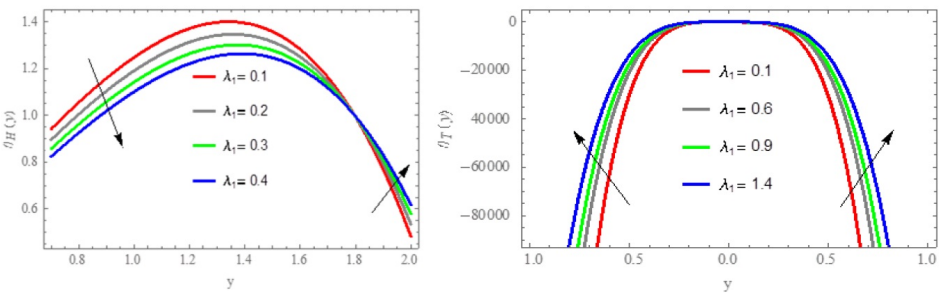


Figure 5: Temperature profile with various values of  $\lambda_1$  at  $\{Fr = 1.5, Re = 1.5, x = 0.1, \alpha = 0.1, \epsilon = 0.3, Q = 1.3, \Phi = 1.3, \Phi_1 = 1.2, t = 0.1, L_1 = 2.1, Pr = 1., Ec_T = 1.1, B = 0.01\}$ : (a) uniform heat flux condition; (b) uniform surface temperature

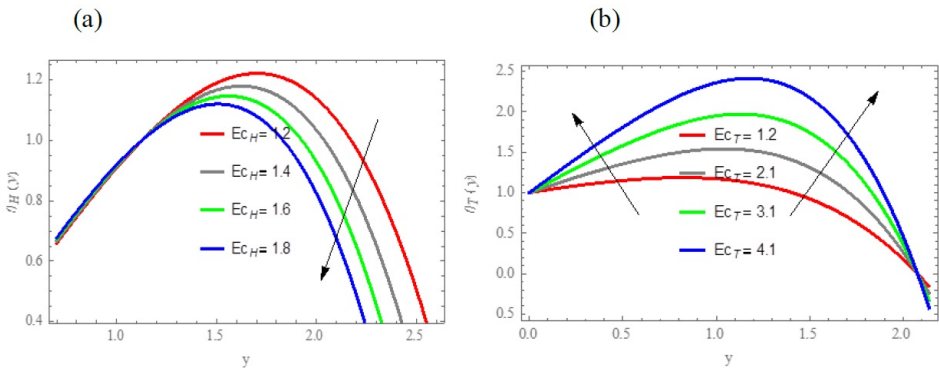


Figure 6: Temperature profile with various values of  $Ec$  at  $\{Fr = 1.5, Re = 1.5, x = 0.4, \alpha = 0.1, \lambda_1 = 0.2, \epsilon = 0.1, Q = 1.3, \Phi = 1.1, \Phi_1 = 0.3, t = 0.1, L_1 = 1.1, Pr = 1.2, B = 0.3\}$ :(a) uniform heat flux condition; (b) uniform surface temperature

### 4.3 pressure gradient $dp/dx$

Figures 7(a)-(d) show the impact of the parameters Reynolds number  $Re$ , the angle inclination of channel  $\alpha$ , the flow rate  $Q$  and roughness parameter  $\Phi_1$  on the pressure gradient  $dp/dx$  behaviour. As seen in Figures 7(a), and 7(b), the rising values of  $Re$  and  $\alpha$  cause an increase in the magnitude of  $dp/dx$  along the whole length of the channel. In addition, the influence of  $Q$  on the magnitude of  $dp/dx$  in Figure 7(c) demonstrates the reduction in  $dp/dx$  magnitude due to an increase in the value of  $Q$ . However, Figure 7(d) shows that there is no influence of  $\Phi_1$  on  $dp/dx$  in the centre region, but the sides show a decrease in  $dp/dx$  values with an enormous deal of  $\Phi_1$ .

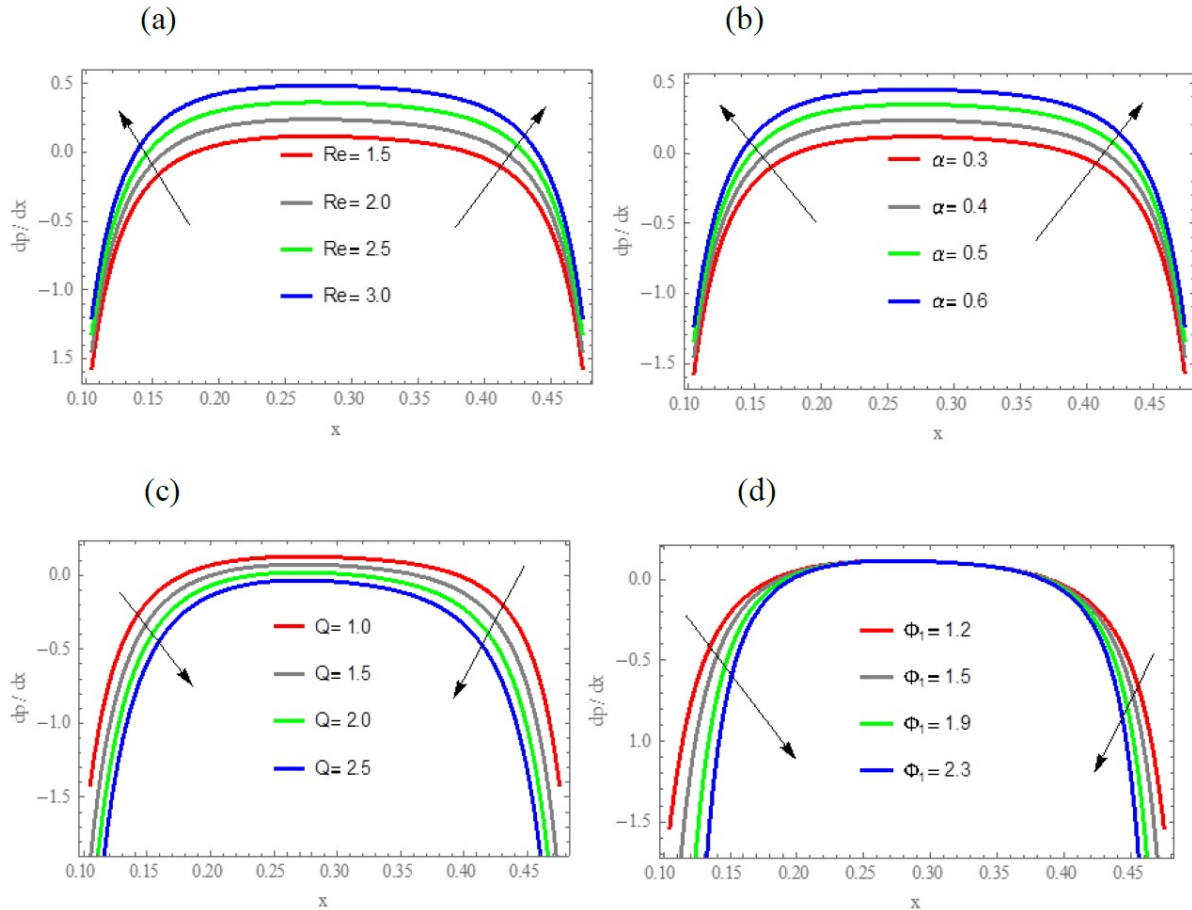


Figure 7: pressure gradient  $dp/dx$  with various values of (a) the Reynolds number  $Re$  (b) the angle inclination of channel  $\alpha$  (c) the flow rate  $Q$  (d) roughness parameter  $\Phi_1$  and for fixed values of parameters  $\{Fr = 1.2, y = 0.4, \lambda_1 = 1.3, \epsilon = 0.3, \Phi = 1.3, t = 0.01, L_1 = 0.61\}$

### 4.4 pressure rise ( $\Delta P$ )

Figures 8(a)-(d) show the pressure rise vs flow rate for different values of the roughness parameter for non-uniform channels. These figures illustrate a linear relationship between pressure rise and flow rate. To employ the peristaltic wave as a pump, it is widely known that pressure rise should occur in the direction of flow ( $\Delta P > 0, Q > 0$ ) while the retrograde pumping achieved for ( $\Delta p_\lambda > 0, Q < 0$ ). For all magnitudes of the surface roughness parameter and various Froude number  $Fr$ , the magnitude of the pressure rise and retrograde flow reduce linearly with an increase in  $Fr$  as seen in Figure 8(a). The Reynolds number  $Re$  has a significant impact on the pressure rise. Figure 8(b) shows that at greater levels magnitudes of  $Re$  a magnitude of the pressure rise (peristaltic and retrograde flow) is visualized as a fast augment. Figures 8(c) and 8(d) depict the variation in pressure rise against flow rate at different values of Jeffrey fluid parameter  $\lambda_1$  and surface roughness parameters  $\Phi_1$ , respectively. It is evident from Figures 8(c) that an increase in Jeffrey fluid parameter  $\lambda_1$ , the peristaltic flow enhances for ( $\Delta P > 0, Q > 0$ ), whereas dumping in the retrograde pumping region ( $\Delta p_\lambda > 0, Q < 0$ ) is noticed. The situation will be reversed in Figure 8(d) with an increase in the value of the surface roughness parameter  $\Phi_1$ . Furthermore, a free pumping ( $\Delta P = 0$ ) appears for ascending values of  $\lambda_1$  and  $\Phi_1$ .

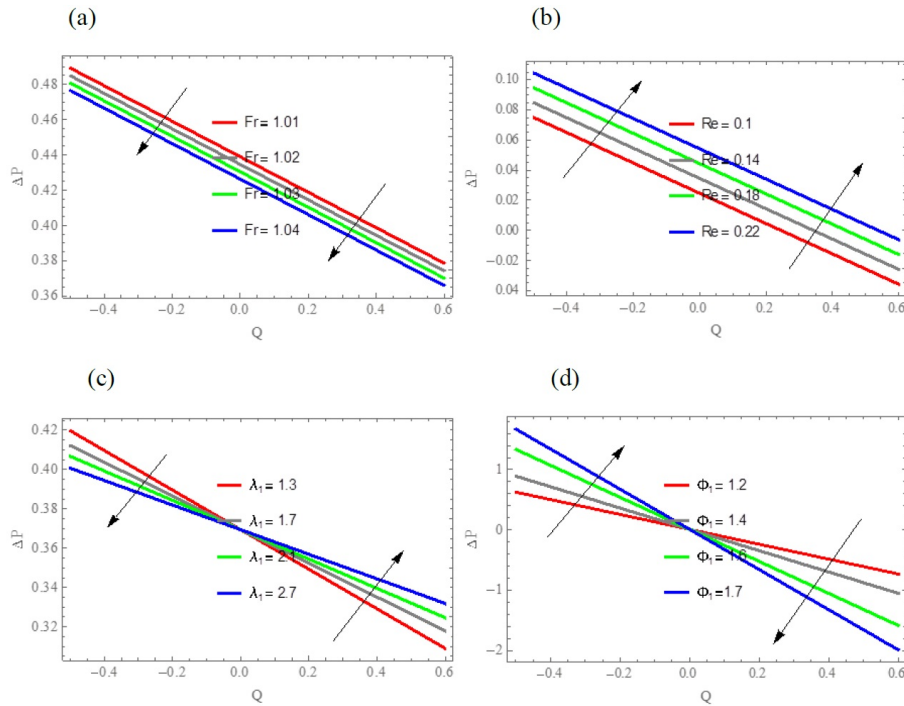


Figure 8: pressure rise ( $\Delta P$ ) with various values of (a) Froude number  $Fr$  (b) Reynolds number  $Re$  (c) Jeffrey fluid parameter  $\lambda_1$  (d) roughness parameter  $\Phi_1$  and for fixed values of parameters  $\{y = 0.4, \alpha = 0.01, \lambda_1 = 1.3, \epsilon = 0.3, x = 0.3, \Phi = 1.3, t = 0.01, L_1 = 0.61, L = 0.61\}$

### 4.5 Trapping Phenomena

The phenomena of trapping (bolus generated owing to streamline splitting) are well-known in peristaltic investigations. The trapped fluid within the bolus is forced forward by the peristaltic wave. Figures 9,10,11,12,13 are presented to illustrate the behaviour of different parameters on streamlines via non-uniformity of the wall  $\epsilon$ , flow rate  $Q$ , amplitude ratio  $\Phi$ , roughness parameter  $\Phi_1$  and wavelength  $L_1$ . The action of non-uniformity of the wall  $\epsilon$  on the trapped bolus is recorded in Figure 9. The magnitude of the trapping bolus diminished in size, and more bolus and streamlines were created. Figure 10 demonstrates that when the value of  $Q$  increases, the amplitude of the trapped bolus increases which is normal because of increasing in fluid moving while the number of bolus remains constant, Figure 11 shows flow behaviour as a function of amplitude ratio  $\Phi$  variation, in which the amplitude of the trapped bolus increases while the number of bolus remains constant. Figure 12 shows the effect of the roughness parameter  $\Phi_1$  on the trapped bolus. Which have the same effect  $\Phi$  and  $Q$ . The size of the trapped bolus decreases as the effect of wavelength  $L_1$  on the flow increases as seen in Figure 13.

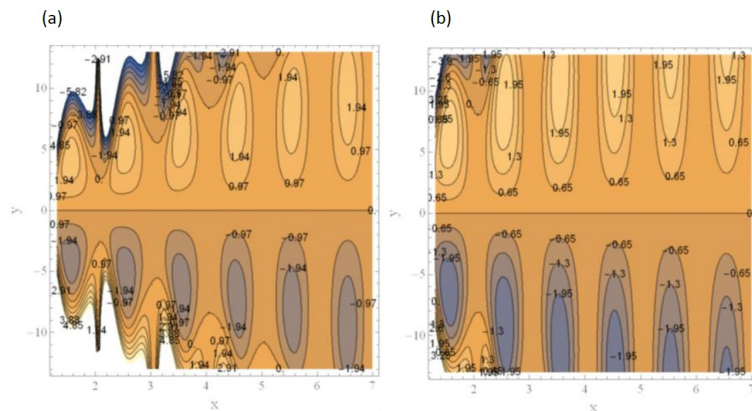


Figure 9: Stream function with various values of non-uniformity of the wall  $\epsilon = \{1.3, 2.8\}$  and for fixed values of parameters  $\{Fr = 1.2, Re = 0.3, \alpha = 0.3, \lambda_1 = 0.3, Q = 1.3, \Phi = 1.3, \Phi_1 = 1.2, t = 0.3, L_1 = 1.1\}$

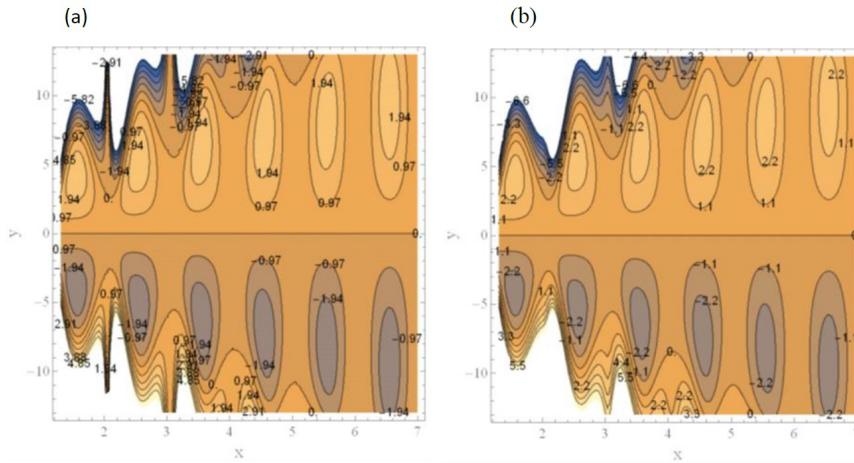


Figure 10: Stream function with various values of flow rate  $Q = \{1.3, 1.5\}$  and for fixed values of parameters  $\{Fr = 1.2, Re = 0.3, \alpha = 0.3, \lambda_1 = 0.3, \epsilon = 1.3, \Phi = 1.3, \Phi_1 = 1.2, t = 0.3, L_1 = 1.1\}$

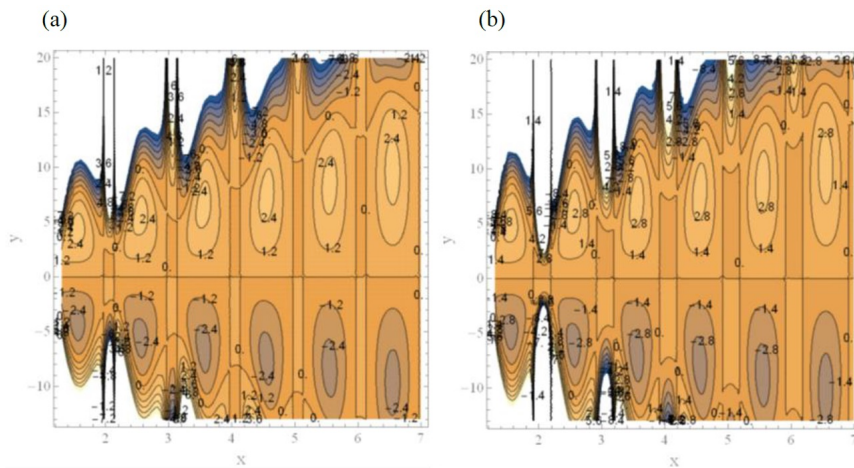


Figure 11: Stream function with various values of amplitude ratio  $\Phi = \{1.0, 1.5\}$  and for fixed values of parameters  $\{Fr = 1.2, Re = 0.3, \alpha = 0.3, \lambda_1 = 0.3, \epsilon = 1.3, Q = 1.3, \Phi_1 = 1.3, t = 0.3, L_1 = 1.1\}$

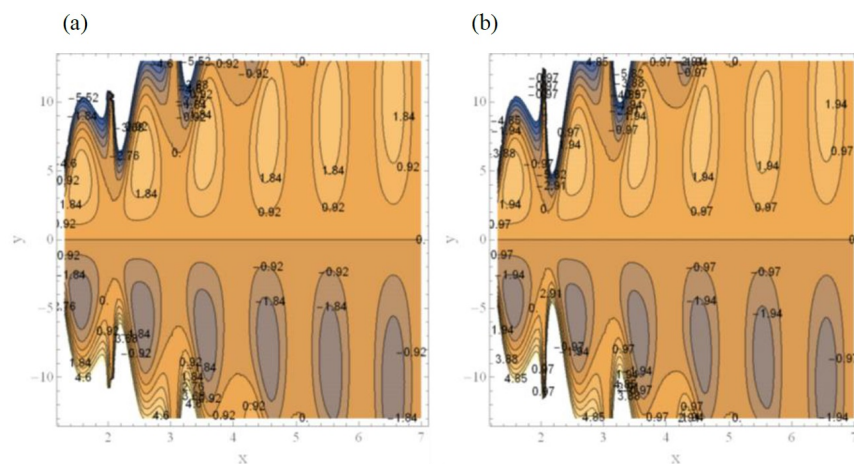


Figure 12: Stream function with various values of roughness parameter  $\Phi_1 = \{1.0, 1.5\}$  and for fixed values of parameters  $\{Fr = 1.2, Re = 0.3, \alpha = 0.3, \lambda_1 = 0.3, \epsilon = 1.5, Q = 1.3, \Phi = 1.3, t = 0.3, L_1 = 1.1\}$

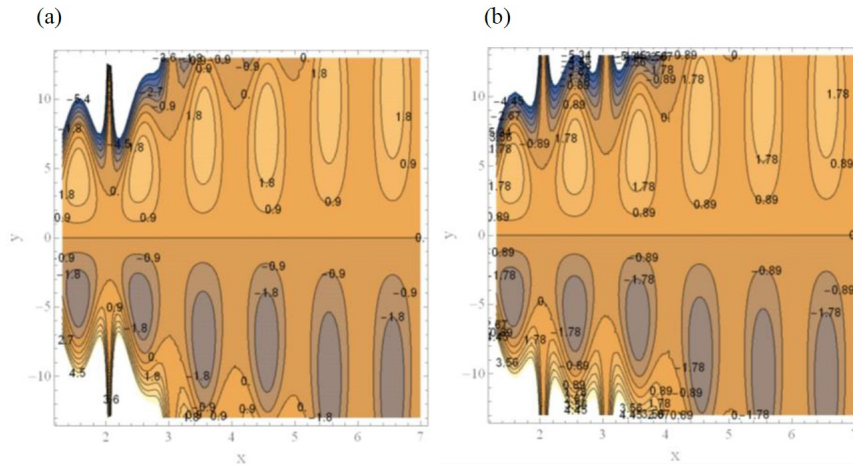


Figure 13: Stream function with various values of wavelength  $L_1 = \{1.1, 3.5\}$  and for fixed values of parameters  $\{Fr = 1.2, Re = 0.3, \alpha = 0.3, \lambda_1 = 0.3, \epsilon = 1.5, Q = 1.3, \Phi = 1.3, \Phi_1 = 1.3, t = 0.3\}$

## 5 Conclusion

The effect of surface roughness on the peristaltic motion of a non-Newtonian Jeffrey fluid down a non-uniform inclined channel is investigated in this work using a novel mathematical approach. The velocity field temperature, pressure gradient, and pressure rise all have an identical solution. The findings of the research are summarized below.

1. Velocity has a parabolic distribution in nature, rising in the centre region of the channel, and the Jeffrey fluid parameter  $\lambda_1$  does not affect Velocity. the influence of the flow rate, The increase in flow rate  $Q$  causes an increase in activity in the central section of the channel and an increase in outcome near the walls.
2. The effect of the roughness parameter  $\Phi_1$  causes the opposite behaviour. The influence of the roughness parameter results in an increasing action in the centre portion of the channel and a reduction near the walls, whereas the effect of amplitude ratio  $\Phi$  results in a decreasing action in the central part of the channel and an increase near the walls. Reverse the roughness parameter's effect.
3. The effect of Jeffrey fluid parameter and amplitude ratio shows that the temperature distribution  $\theta_H(y)$ ,  $\theta_T(y)$  has the opposite behaviour. An increase in the right side of the channel and a decrease in the left side of the channel walls. however, the effect of  $\Phi_1$  on  $\theta_H(y)$ ,  $\theta_T(y)$  have the same impact from the left side of the channel wall, but there is a difference in the size of the drop, as when the roughness parameter decreases by a high percentage, and when the Eckert number increases, it decreases slightly.
4. Increasing Reynolds number  $Re$  and the angle inclination of channel  $\alpha$  raises the magnitude of the pressure gradient  $dp/dx$ , whereas it reduces as the flow rate  $Q$  and roughness parameter  $\Phi_1$  increases,
5. Reynolds number  $Re$  increasing, the magnitude of the peristaltic pumping ( $\Delta P > 0, Q > 0$ ) grows, but it decreases as the Froude number  $Fr$  increases, while the opposite effect for Jeffrey fluid parameter  $\lambda_1$  and roughness parameter  $\Phi_1$  on the pumping and retrograde pumping is seen.
6. The size of the trapping bolus decreases upon an increment of non-uniformity of the wall  $\epsilon$ , while increases in number, however, remains unchanged in a number of boluses with decreases in The size of the trapping bolus upon an increment of wavelength  $L_1$ .
7. The trapped bolus enlarged in size and while unchanged in a number of boluses when flow rate  $Q$ , roughness parameter  $\Phi_1$  and amplitude ratio  $\Phi$  enhances.

## References

- [1] Z. Abbas, M.Y. Rafiq, J. Hasnain and T. Javed, *Peristaltic transport of a Casson fluid in a non-uniform inclined tube with Rosseland approximation and wall properties*, Arabian J. Sci. Eng. **46** (2021), no. 3, 1997–2007.
- [2] F.M. Abbasi, S.A. Shehzad, T. Hayat and M.S. Alhuthali, *Mixed convection flow of Jeffrey nanofluid with thermal radiation and double stratification*, J. Hydrodynamics, Ser. B. **28** (2016), no. 5, 840–849.
- [3] N.S. Akbar, S. Nadeem and C. Lee, *Characteristics of Jeffrey fluid model for peristaltic flow of chyme in small intestine with magnetic field*, Results Phys. **3** (2013), 152–160.

- [4] N.S. Akbar, S. Nadeem, C. Lee, Z. Hayat Khan and R. Ul Haq, *Numerical study of Williamson nanofluid flow in an asymmetric channel*, Results Phys. **3** (2013), 161–166.
- [5] S. Akram and S. Nadeem, *Influence of induced magnetic field and heat transfer on the peristaltic motion of a Jeffrey fluid in an asymmetric channel: closed form solutions*, J. Magnetism Magnetic Mater. **328** (2013), 11–20.
- [6] N. Ali, M. Sajid, Z. Abbas and T. Javed, *Non-Newtonian fluid flow induced by peristaltic waves in a curved channel*, Eur. J. Mech.-B/Fluids **29** (2010), no. 5, 387–394.
- [7] M. Asgir, A.A. Zafar, A.M. Alsharif, M.B. Riaz and M. Abbas, *Special function form exact solutions for Jeffery fluid: an application of power law kernel*, Adv. Differ. Equ. **2021** (2021), no. 1, 1–18.
- [8] B.B. Gupta and V. Seshadri, *Peristaltic pumping in non-uniform tubes*, J. Biomech. **9** (1976), no. 2, 105–109.
- [9] D.A.H. Hanaor, Y. Gan and I. Einav, *Static friction at fractal interfaces*, Tribology Int. **93** (2016), 229–238.
- [10] T. Hayat, Y. Wang, K. Hutter, S. Asghar and A.M. Siddiqui, *Peristaltic transport of an Oldroyd-B fluid in a planar channel*, Math. Prob. Engin. **2004** (2004), no. 4, 347–376.
- [11] T. Hayat, Y. Wang, A.M. Siddiqui and K. Hutter, *Peristaltic motion of a Johnson-Segalman fluid in a planar channel*, Math. Prob. Engin. **2003** (2003), no. 1, 1–23.
- [12] T. Hayat, Y. Wang, A.M. Siddiqui, K. Hutter and S. Asghar, *Peristaltic transport of a third-order fluid in a circular cylindrical tube*, Math. Models Meth. Appl. Sci. **12** (2002), no. 12, 1691–1706.
- [13] T. Hayat, H. Zahir, A. Tanveer and A. Alsaedi, *Soret and Dufour effects on MHD peristaltic transport of Jeffrey fluid in a curved channel with convective boundary conditions*, PLoS ONE **12** (2017), no. 2, p. 0164854.
- [14] P. Lakshminarayana, S. Sreenadh, G. Sucharitha and K. Nandgopal, *Effect of slip and heat transfer on peristaltic transport of a Jeffrey fluid in a vertical asymmetric porous channel*, Adv. Appl. Sci. Res. **6** (2015), no. 2, 107–118.
- [15] T.W. Latham, *Fluid motions in a peristaltic pump*, PhD diss. Massachusetts Institute of Technology, 1966.
- [16] K.S. Mekheimer, *Peristaltic transport of a couple stress fluid in a uniform and non-uniform channels*, Biorheology **39** (2002), no. 6, 755–765.
- [17] K.S. Mekheimer, *Peristaltic flow of blood under effect of a magnetic field in a non-uniform channels*, Appl. Math. Comput. **153** (2004), no. 3, 763–777.
- [18] K.S. Mekheimer, E.F. El Shehawey and A.M. Elaw, *Peristaltic motion of a particle-fluid suspension in a planar channel*, Int. J. Theor. Phys. **37** (1998), no. 11, 2895–2920.
- [19] A. Movassagh, X. Zhang, E. Arjomand and M. Haghighi, *A comparison of fractal methods for evaluation of hydraulic fracturing surface roughness*, APPEA J. **60** (2020), no. 1, 184–196.
- [20] S. Nadeem and N.S. Akbar, *Influence of heat transfer on a peristaltic transport of Herschel–Bulkley fluid in a non-uniform inclined tube*, Commun. Nonlinear Sci. Numerical Simul. **14** (2009), no. 12, 4100–4113.
- [21] N.E. Odling, *Natural fracture profiles, fractal dimension and joint roughness coefficients*, Rock Mech. Rock Engin. **27** (1994), no. 3, 135–153.
- [22] N.V. Priezjev, *Effect of surface roughness on rate-dependent slip in simple fluids*, J. Chem. Phys. **127** (2007), no. 14, p. 144708.
- [23] K. Ramesh, *Effects of viscous dissipation and Joule heating on the Couette and Poiseuille flows of a Jeffrey fluid with slip boundary conditions*, Propulsion Power Res. **7** (2018), no. 4, 329–341.
- [24] M.G. Reddy and O.D. Makinde, *Magnetohydrodynamic peristaltic transport of Jeffrey nanofluid in an asymmetric channel*, J. Molecular Liquids **223** (2016), 1242–1248.
- [25] M.R. Salman and H.A. Ali, *Approximate treatment for the MHD peristaltic transport of Jeffrey fluid in inclined tapered asymmetric channel with effects of heat transfer and porous medium*, Iraqi J. Sci. **2020** (2020), 3342–3354.
- [26] A.H. Shapiro, M.Y. Jaffrin and S.L. Weinberg, *Peristaltic pumping with long wavelengths at low Reynolds number*, J. Fluid Mech. **37** (1969), no. 4, 799–825.
- [27] R. Shukla, S.S. Bhatt, A. Medhavi and R. Kumar, *Effect of surface roughness during peristaltic movement in a*

- nonuniform channel*, Math. Prob. Engin. **2020** (2020).
- [28] A.M. Siddiqui and W.H. Schwarz, *Peristaltic motion of a third-order fluid in a planar channel*, Rheologica Acta **32** (1993), no. 1, 47–56.
- [29] A.M. Siddiqui and W.H. Schwarz, *Peristaltic flow of a second-order fluid in tubes*, J. Non-Newtonian Fluid Mech. **53** (1994), 257–284.
- [30] K. Vajravelu, S. Sreenadh, G. Sucharitha and P. Lakshminarayana, *Peristaltic transport of a conducting Jeffrey fluid in an inclined asymmetric channel*, Int. J. Biomath. **7** (2014), no. 6, 1450064.
- [31] D.B. Van Dam and C.J. De Pater, *Roughness of hydraulic fractures: importance of in-situ stress and tip processes*, Spe J. **6** (2001), no. 1, 4–13.
- [32] Y. Wang, T. Hayat and K. Hutter, *Peristaltic flow of a Johnson-Segalman fluid through a deformable tube*, Theore. Comput. Fluid Dyn. **21** (2007), no. 5, 369–380.
- [33] C. Zhai, Y. Gan, D. Hanaor, G. Proust and D. Retraint, *The role of surface structure in normal contact stiffness*, Experim. Mech. **56** (2016), no. 3, 359–368.